RSC Advances

PAPER

View Article Online
View Journal | View Issue

Cite this: *RSC Adv.*, 2015, **5**, 16234

Nanoscale phase separation control in rationally designed conjugated polymer solar cells processed using co-additives†

Xichang Bao, Liang Sun, Chuantao Gu, Zhengkun Du, Shuguang Wen, Ting Wang, Ning Wang and Renqiang Yang*

Received 14th November 2014
Accepted 26th January 2015

DOI: 10.1039/c4ra14522d

www.rsc.org/advances

A conjugated polymer based on benzo[1,2-*b*:4,5-*b*′]dithiophene with a thiophene-conjugated side chain and *N*-alkylthieno[3,4-*c*]pyrrole-4,6-dione was synthesized. When shortening the alkyl to linear hexyl on thiophene, the polymer (PBDT2T6–TPD) still has good solubility in common solvents and the hole mobility is improved. By introducing two additives (1,8-diiodooctane and 1,6-dibromohexane) as co-additives in chlorobenzene solution, a nanoscale phase separation with excellent bicontinuous interpenetrating network and balanced hole mobility and electron mobility was obtained in the blend film of PBDT2T6–TPD and [6,6]-phenyl C61 butyric acid methyl ester. Combined with an appropriate side chain of polymer and post-processing of the device, the solar cells exhibit a power conversion efficiency of 6.73% with a remarkable short circuit current density of 12.91 mA cm^{-2}.

Introduction

Polymer solar cells (PSCs) have attracted more and more attention as a renewable energy source owing to their advantages of easy fabrication, low cost, light weight, and the possibility to fabricate on flexible substrates.[1–3] PSCs are prepared from a blend of an electron donor (p-type conjugated polymers) and an electron acceptor (n-type fullerene derivatives) as the active layer. Recently, through developing low band gap polymers and device engineering, great advances have been made.[4–10] However; the major obstacle for its commercial application is still the relatively low efficiency and poor device stability, which urge scientists to explore new materials and device technology.

An ideal polymer donor in PSCs should exhibit broad absorption, high hole mobility, suitable electronic energy level matching with the fullerene acceptor, and good compatibility with the fullerene acceptor to form an appropriate nanoscale. One of the most effective strategies is to design polymers containing alternating donor (D) and acceptor (A) units in the backbone or side chains.[7–14] Benzo[1,2-*b*:4,5-*b*′]dithiophene (BDT) as one of the most efficient donor units has been used to construct efficient D–A copolymers. For example, Hou designed and synthesized a series of two-dimensional (2D) conjugated BDT based polymers with a conjugated side chain, which possess higher hole mobility and broader absorption. The polymers demonstrated good device performance in PSCs.[12] Among the variety of electron deficient units, *N*-alkylthieno[3,4-*c*]pyrrole-4,6-dione (TPD) has attracted much attention for its special property of controlling the energy levels for D–A conjugated copolymers.[15–17] Ma *et al.* presented a PBDT-2T8–TPD copolymer with an alkylthienyl side chains which demonstrated a power conversion efficiency (PCE) of 6.17% with the short circuit current density (J_{SC}) of 9.79%.[17] As previous report by Kim *et al.*,[18] ensuring the solubility and reducing the length of the side chains could increase π–π stacking, thus improve the performance of organic electronics. Taking into account all these recent results, polymer with much short side chain needs to be further investigated.

Furthermore, for device engineering, inverted PSCs with high-work-function metals (Au, Ag) covering on stable metal oxide interfacial layers (generally molybdenum oxide, MoO_3 (ref. 19 and 22)) as top anode, and n-type metal oxides, zinc oxide (ZnO),[19,20] titanium oxide (TiO_X),[21,22] modified indium tin oxide (ITO) coated glass as the cathode, could avoid the stability problem of conventional solar cells. Among the n-type metal oxides, ZnO is an ideal electron transport layer with wide band gap, high transmission in the visible wavelength range and good positioning of the conduction band (−4.4 eV) in combination with [6,6]-phenyl C61 butyric acid methyl ester ($PC_{61}BM$).[23] Moreover, control of the morphology of the active layer is of paramount importance in achieving high-efficiency solar cells because it directly affects photocurrent.[24–26] By incorporating a small amount of specific processing additives, such as 1,8-diiodooctane (DIO), into the host solvent, it is

CAS Key Laboratory of Bio-based Materials, Qingdao Institute of Bioenergy and Bioprocess Technology, Chinese Academy of Sciences, Qingdao 266101, China. E-mail: yangrq@qibebt.ac.cn; Fax: +86-532-80662778; Tel: +86-532-80662700

† Electronic supplementary information (ESI) available: Details of synthesis, device fabrication, TGA curves, and device with different conditions. See DOI: 10.1039/c4ra14522d

possible to control the phase separation in active layer and improve the performances of the devices.[27,28] Recently, co-additives was more effective than single processing additive, it becomes a much more useful method to control the morphology of active layers.[29,30]

In this work, we made a slight modification and the polymer PBDT2T6–TPD containing a 2D monomer BDT with a short linear C6 side chain on thiophene as the donor and TPD with a ethylhexyl side chain as the acceptor was synthesized, which also demonstrated good solubility in common solvents. The hole mobility was improved to 1.18×10^{-4} cm^2 V^{-1} s^{-1} as our expected. Next, through processed with co-additives in morphology, a good nanoscale phase separation with excellent bicontinuous interpenetrating network was formed and the hole/electron transport became much more balance in the active layer. Finally, combined with polymer design and device processing optimization, the inverted PBDT2T6–TPD:$PC_{61}BM$ based solar cell exhibits a high PCE of 6.73% with a remarkable short circuit current density (J_{SC}) of 12.91 mA cm^{-2}.

Results and discussion

2.1 Polymer synthesis and characterization

The synthetic routes are illustrated in Scheme S1† and the structure is shown in the inset of Fig. 1. The monomer TPD and BDT2T6 were prepared according to the published procedures.[31,32] PBDT2T6–TPD was synthesized by Stille coupling between bis(trimethyl)stannane of BDT2T6 and dibromides of TPD using $Pd_2(dba)_3$/P(*o*-tol)$_3$ as the catalyst. The obtained polymer was purified by silica gel column chromatography using chloroform as the eluent, and then precipitated in methanol. The presence of branched C8 side chain on the TPD unit enhanced the solubility of the resulting polymers, while conjugated side chains possess higher hole mobility which attributes to the 2D-conjugated structure. The number-average (14 kDa) and weight-average (32 kDa) molecular weights were obtained from gel permeation chromatography (GPC) using tetrahydrofuran (THF) as the eluent. The polymer exhibits good solubility in commonly used solvents, such as chloroform (CF), chlorobenzene (CB) and *o*-dichlorobenzene (*o*-DCB). The linear C6 alkylthienyl side chains on the BDT unit shows preferable properties in comparison with C8 alkylthienyl side chains. The thermal stability of PBDT2T6–TPD copolymer was measured by thermogravimetric analysis (TGA) under a N_2 flow, and the result showed that the decomposition temperature with 5% weight loss is 435 °C (Fig. S1†), indicating a good thermal stability for photovoltaic application.

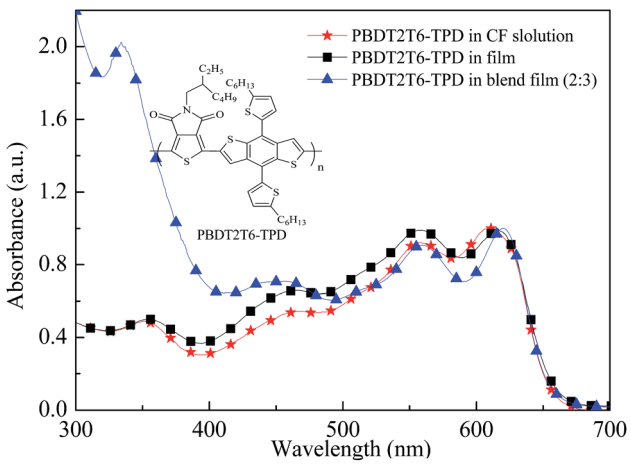

Fig. 1 UV-vis spectra of the polymer PBDT2T6–TPD in $CHCl_3$ solution, pure film, and PBDT2T6–TPD : $PC_{61}BM$ (2 : 3) blend film.

2.2 Optical and electrochemical properties

Ultraviolet-visible (UV-vis) absorption spectra of PBDT2T6–TPD in diluted chloroform solution, thin film, and PBDT2T6–TPD:$PC_{61}BM$ blend film are shown in Fig. 1. In dilute chloroform solution and in film, the polymer shows a broad absorption. There are two absorption peaks, which is a common feature of D–A type copolymers. The absorption peak at short wavelength is originated from π–π* transition of the conjugated polymer backbone. The peak at long wavelength could be attributed to the strong intramolecular charge transfer (ICT) between the electron-rich moieties and electron-deficient segments in the polymer backbone.[33] The absorption of PBDT2T6–TPD in solution is almost the same as the one in film with an absorption onset at 665 nm, which could be a certain degree of packing formed even in the diluted solution. The optical band gap of the polymer is about 1.86 eV calculated from the onset. Interestingly, the absorption at short wavelengths in film is stronger than that in solution, indicating the enhancement of π–π stacking in film.

Cyclic voltammetry (CV) was performed to investigate the redox behaviour of the polymer and deduce the highest occupied molecular orbit (HOMO) and the lowest unoccupied molecular orbit (LUMO) energy levels of the polymer. The HOMO and LUMO energy levels were determined by measuring the onset oxidation potential (E_{ox}) and onset reduction potential (E_{red}) of the polymer film. Here, the CV measurement was performed on a CHI660D electrochemical workstation with a three-electrode system. Glassy carbon electrode, platinum wire and saturated calomel electrode (SCE) were used as working, counter and reference electrodes, respectively. The measurement was done in anhydrous acetonitrile containing 0.1 M tetra-*n*-butylammonium hexafluorophosphate (*n*-Bu_4NPF_6) as a supporting electrolyte under argon atmosphere at a scan rate of 100 mV s^{-1}. A thin film was deposited from chloroform solution on the working electrode and dried under nitrogen prior to measurement. The redox potential of the Fc/Fc^+ internal reference is 0.38 V *vs.* SCE. The HOMO and LUMO energy levels were determined according to the empirical equation $E_{HOMO} = -e(E_{ox} + 4.8 - E_{1/2,(Fc/Fc^+)})$ eV and $E_{LUMO} = -(E_{red} + 4.8 - E_{1/2,(Fc/Fc^+)})$ eV, where E_{ox} and E_{red} were the onset oxidation potential and onset reduction potential, respectively.[34]

As shown in Fig. 2, PBDT2T6–TPD exhibits reversible reduction and oxidation behaviour. The onsets of oxidation and reduction of PBDT2T6–TPD were observed at +0.95 and −1.09 V *vs.* SCE, accordingly, the HOMO and LUMO levels were at −5.36 and −3.32 eV. The electrochemical band gap calculated from

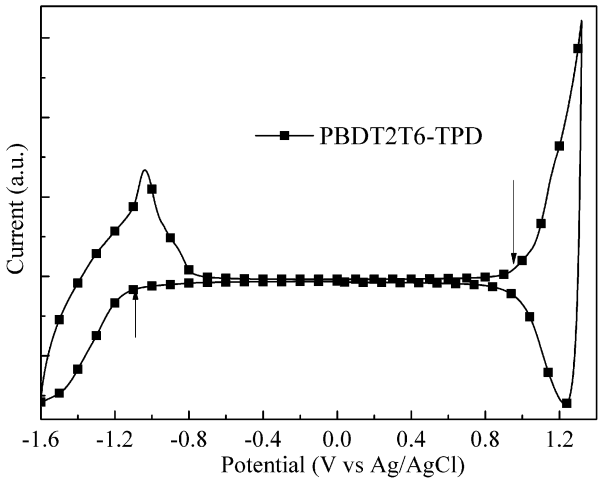

Fig. 2 Cyclic voltammogram of the polymer PBDT2T6–TPD film.

the HOMO and LUMO energy levels is 2.04 eV, 0.18 eV higher than the optical band gap, which might result from the interface barrier between the polymer film and the electrode surface.[35]

2.3 Photovoltaic properties

To demonstrate potential application of the polymer in PSCs, we used PBDT2T6–TPD as an electron donor and $PC_{61}BM$ as an electron acceptor to fabricate bulk heterojunction PSCs with a structure of ITO/ZnO/PBDT2T6–TPD:$PC_{61}BM$/MoO_3/Ag under the illumination of AM 1.5G at 100 mA cm^{-2}. Our previous results showed that 1,6-dibromohexane (DBH) is a good additive can improve solar cell performance.[36] Here, DBH and DIO were chosen as co-additives in the CB solution of PBDT2T6–TPD and $PC_{61}BM$ to control the morphology and phase separation. The chlorobenzene, additives DBH and DIO show an interesting phenomenon, the boiling points have a gradient increased value of about 100 °C. The typical current density–voltage curves are shown in Fig. 3 and the detail device parameters under different conditions are summarized in Table S1.† All devices show relatively high V_{OC} as expected, and the V_{OC} slightly deceases from 0.95 V to 0.89 V as decreasing the donor/acceptor weight ratio from 1 : 1 to 1 : 3. This could be due to the increasing $PC_{61}BM$ in the blend stabilizes the charge transfer state by lowering the effective LUMO level of $PC_{61}BM$ through the formation of $PC_{61}BM$ clusters.[37] The device at weight ratio of 2 : 3 gives the best performance, and the V_{OC}, J_{SC}, FF and PCE are 0.95 V, 10.58 mA cm^{-2}, 48.74% and 4.88%, respectively. Meanwhile, a control conventional structure with a weight ratio of 2 : 3 was also prepared and the PCE is only 4.11%. According to ref. 17, the J_{SC} values of the PSCs using similar polymers with longer alkylthienyl side chains are in the range of 5.90–8.18 mA cm^{-2}, lower than the value reported here. The improved J_{SC} could be due to increased π–π stacking of the designed polymer. With the introducing of the additive, the photovoltaic performance was improved. After addition of 5% (v/v) DIO, the PCE reached 5.94%, with a V_{OC} of 0.89 V, a J_{SC} of 12.24 mA cm^{-2},

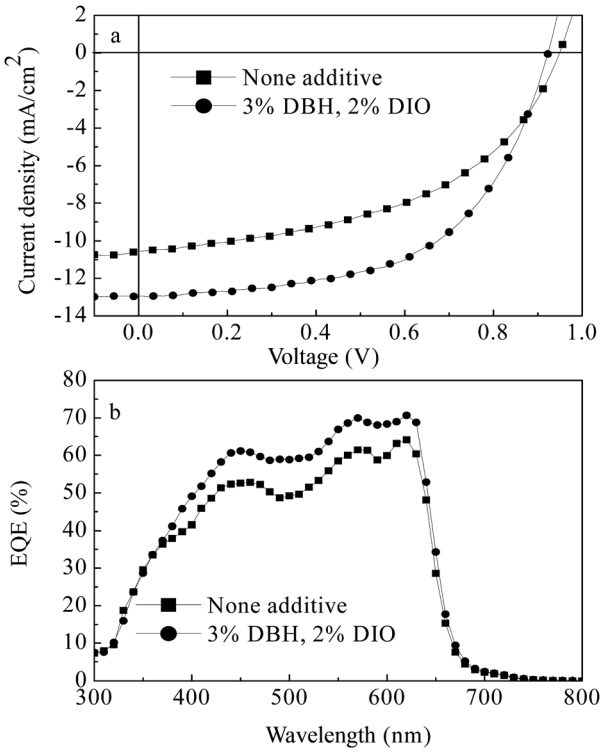

Fig. 3 Typical *J*–*V* curves and related EQE spectra.

and a FF of 55.02%. Meanwhile, when the addition changed to 5% (v/v) DBH, the PCE reached 6.00%, with a V_{OC} of 0.90 V, a J_{SC} of 11.87 mA cm^{-2}, and a FF of 56.17%. The improved device efficiency is due to the enhanced J_{SC} for form better nanoscale phase separation in active layer with appropriate additives. However, the processing additive result in the corresponding drop in V_{OC}. This could be due to the introduction of additive induce the aggregation of the polymer, which increases the effective HOMO level of the polymer and leads to the shift in charge transfer energy.[37] Interestingly, the photovoltaic performance was further improved when using co-additives. The J_{SC} and PCE are increased to 12.91 mA cm^{-2} and 6.73% (Fig. 3). The further improved device performance is due to control at the same time the $PC_{61}BM$ domain and the active layer nanoscale morphology for low solubility conjugated polymer by using co-additives.[29] To evaluate the effect of the additives on the J_{SC}, two external quantum efficiencies (EQE) were measured and shown in Fig. 3(b). The EQE spectrum of the co-additives processed device is higher than the additive-free one in the whole absorption range and the highest value is 70% at 650 nm. The J_{SC} calculated from the EQE spectra are well consistent with those obtained from *J*–*V* curves.

2.4 Morphology characterization

To further understand the improved photovoltaic properties of the resulting polymer and the effects of the additives, the surface morphologies and phase images of the polymer/$PC_{61}BM$ blend films were measured with tapping mode atomic force microscopy (AFM) and the results are shown in Fig. 4. All films

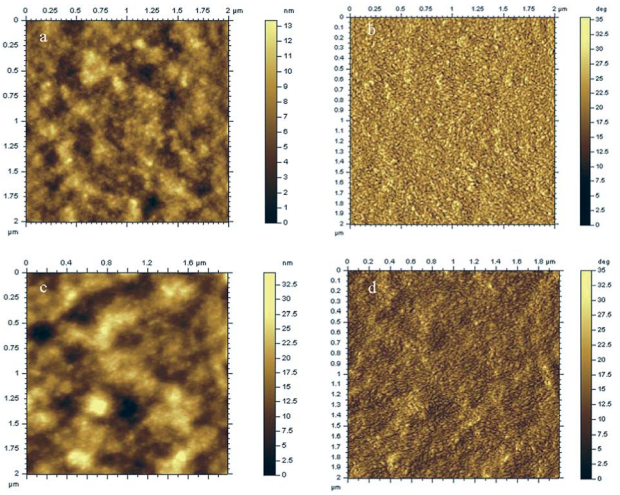

Fig. 4 AFM surface morphologies (left) and phase images (right) for PBDT2T6–TPD/$PC_{61}BM$ blend films (2 : 3), top without additives; bottom with optimized additives. The scanning size is 2 μm × 2 μm.

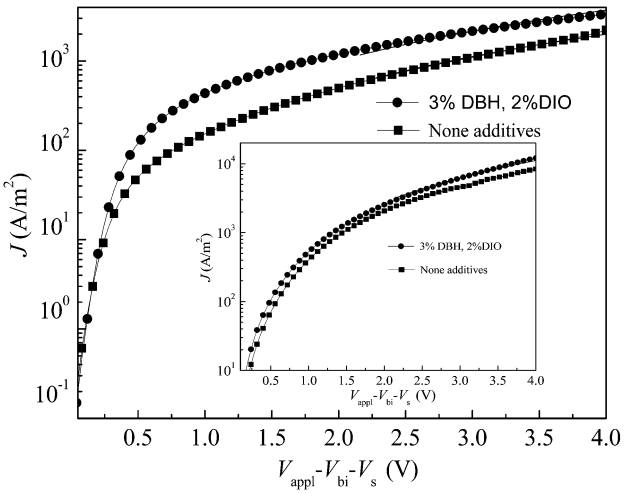

Fig. 5 Hole mobility characteristics of PBDT2T6–TPD and $PC_{61}BM$ (2 : 3) without and with optimized additives. The inset figure is electron mobility.

were prepared under the same conditions as the optimized photovoltaic devices. One can see that the surface of the additive-free blend film is very smooth with a root mean square roughness (RMS) of 1.83 nm (Fig. 4a). As we know that the diffusion length is less than 20 nm and the perfect domain size should not exceed 30 nm.[38] For the phase image, the dark-colored and light-colored areas correspond to $PC_{61}BM$ and polymer domains, respectively. The domain sizes are very uniform of about 40 nm. The additive-free film with good surface morphology and slightly larger domain sizes exhibits a moderate PCE of 4.88% with a relatively high J_{SC} of 10.58 mA cm^{-2}. With the addition of co-additives, the surface of the blend films became rougher and the RMS value is 4.66 nm. Interestingly, a more favourable nanoscale phase separation with the domain size of about ~25 nm was formed. The ideal domain size and excellent bicontinuous interpenetrating network with optimized co-additives effectively improved the separation and charge transport. The PCE up to 6.73% is achieved with greatly improved J_{SC} (from 10.58 mA cm^{-2} of additive-free device to 12.91 mA cm^{-2}).

2.5 Mobility

The hole mobility is another important factor for PSCs due to its direct influence charge transport. High mobility could guarantee effective charge transport to the electrodes and reduce the photocurrent loss in photovoltaic devices. Meanwhile, balanced hole and electron mobilities in the active layer can improve solar cell performance.[39,40] The hole and electron only mobilities of the blend film were measured by space charge limit current (SCLC) theory with a device structure of ITO/PEDOT:PSS/donor:$PC_{61}BM$/MoO_3/Ag for the hole-only and ITO/ZnO/donor:$PC_{61}BM$/Ca/Al for electron-only. The SCLC is described by

$$J_{SCLC} = \frac{9}{8}\varepsilon_0\varepsilon_r\mu\frac{V^2}{L^3} \quad (1)$$

Here, J stands for current density, ε_0 is the permittivity of free space, ε_r is the relative dielectric constant of the transport medium, μ is the hole or electron mobility, V is the internal potential in the device and L is the thickness of the active layer. The internal potential V is obtained by subtracting the built-in voltage (V_{bi}) and the voltage drop (V_s) from the series resistance of the substrate from the applied voltage (V_{appl}), accordingly: $V = V_{appl} - V_{bi} - V_s$. As shown in Fig. 5, according to eqn (1), the hole mobilities without and with optimized additives are calculated to be 7.21 × 10^{-5} cm^2 V^{-1} s^{-1} and 1.18 × 10^{-4} cm^2 V^{-1} s^{-1}. These results are slightly higher than the previous reported values of polymer with longer side chains, which could be due to the increased π–π stacking.[17] The electron mobilities without and with optimized additives are calculated to be 1.74 × 10^{-4} cm^2 V^{-1} s^{-1} and 2.23 × 10^{-4} cm^2 V^{-1} s^{-1}, which is corresponding to the previous reported results.[41] The improved hole and electron mobilities were ascribed to form a much more favorable nanoscale phase separation for charge transport when introducing the co-additives. Moreover, the ratio between hole and electron mobilities is decreased from 2.41 for additive-free active layer to 1.89 for the film with optimized co-additives. The much more balanced hole and electron transport results in high photocurrent and enhanced photovoltaic performance of the device.

Conclusion

In summary, a conjugated polymer based on benzo[1,2-*b*:4,5-*b*′] dithiophene with a thiophene-conjugated side chain and *N*-alkylthieno[3,4-*c*]pyrrole-4,6-dione was synthesized. Although decreasing the alky to linear C6 side chain on thiophene, the polymer (PBDT2T6–TPD) still shows good solubility in common solvents, high decomposition temperature of 435 °C, and improved hole mobility compared to the polymer with longer

alkyl side chain. With introducing two additives (DBH and DIO) as co-additives in chlorobenzene solutions, a nanoscale phase separation with excellent bicontinuous interpenetrating network and more balanced hole mobility and electron mobility were obtained in the blend film of PBDT2T6–TPD:$PC_{61}BM$. Combined with appropriate side chain of polymer and post device processing, the device exhibits a PCE of 6.73% with a remarkable J_{SC} of 12.91 mA cm^{-2}. Our preliminary results show that the PBDT2T6–TPD is a promising donor material and processing with co-additives can further tune the nanoscale phase separation.

Acknowledgements

This work was supported by the National Natural Science Foundation of China (61107090, 51303197, 51173199, 21202181, and 21204097), the Ministry of Science and Technology of China (2014CB643501, 2010DFA52310), and Qingdao Municipal Science and Technology Program (11-2-4-22-hz and 14-2-4-28-jch).

Notes and references

1 S. Gunes, H. Neugebaue and N. S. Saricici, *Chem. Rev.*, 2007, **107**, 1324.
2 J. Chen and Y. Cao, *Acc. Chem. Res.*, 2009, **42**, 1709.
3 Z. B. Henson, K. Mullen and G. C. Bazan, *Nat. Chem.*, 2012, **4**, 699.
4 Z. He, C. Zhong, S. Su, M. Xu, H. Wu and Y. Cao, *Nat. Photonics*, 2012, **6**, 591.
5 J. You, C. Chen, Z. Hong, K. Yoshimura, K. Ohya, R. Xu, S. Ye, J. Gao, G. Li and Y. Yang, *Adv. Mater.*, 2013, **25**, 3973.
6 J. You, L. Dou, K. Yoshimura, T. Kato, K. Ohya, T. Moriarty, K. Emery, C. Chen, J. Gao, G. Li and Y. Yang, *Nat. Commun.*, 2013, **4**, 1446.
7 T. Nguyen, H. Choi, S. Ko, M. Uddin, B. Walker, S. Yum, J. Jeong, M. Yun, T. Shin, S. Hwang, J. Kim and H. Woo, *Energy Environ. Sci.*, 2014, **7**, 3040.
8 C. Gu, M. Xiao, X. Bao, L. Han, D. Zhu, N. Wang, S. Wen, W. Zhu and R. Yang, *Polym. Chem.*, 2014, **5**, 6551.
9 Q. Liu, X. Bao, S. Wen, Z. Du, L. Han, D. Zhu, Y. Chen, M. Sun and R. Yang, *Polym. Chem.*, 2014, **5**, 2076.
10 H. Zhou, L. Yang and W. You, *Macromolecules*, 2012, **45**, 607.
11 M. Zhang, X. Guo, S. Zhang and J. Hou, *Adv. Mater.*, 2014, **26**, 1118.
12 L. Ye, S. Zhang, L. Huo, M. Zhang and J. Hou, *Acc. Chem. Res.*, 2014, **47**, 1595.
13 C. Cui, W. Wong and Y. Li, *Energy Environ. Sci.*, 2014, **7**, 2276.
14 H. Chen, Y. Chen, C. Liu, Y. Chien, S. Chou and P. Chou, *Chem. Mater.*, 2012, **24**, 4766.
15 Y. Zou, A. Najari, P. Berrouard, S. Beaupre, B. R. Aïch, Y. Tao and M. Leclerc, *J. Am. Chem. Soc.*, 2010, **132**, 5330.
16 C. Piliego, T. W. Holcombe, J. D. Douglas, C. H. Woo, P. M. Beaujuge and J. Fréchet, *J. Am. Chem. Soc.*, 2010, **132**, 7595.
17 J. Yuan, Z. Zhai, H. Dong, J. Li, Z. Jiang, Y. Li and W. Ma, *Adv. Funct. Mater.*, 2013, **23**, 885.
18 I. Kang, H. J. Yun, D. S. Chung, S. K. Kwon and Y. H. Kim, *J. Am. Chem. Soc.*, 2013, **135**, 14896.
19 S. Sanchez, S. Berson, S. Guillerez, C. Clement and V. Ivanova, *Adv. Energy Mater.*, 2012, **5**, 541.
20 H. Cheun, C. Hernandez, Y. Zhou, W. Potscavage, S. Kim, J. Shim, A. Dindar and B. Kippelen, *J. Phys. Chem. C*, 2010, **114**, 20713.
21 Z. Lin, C. Jiang, C. Zhu and J. Zhang, *ACS Appl. Mater. Interfaces*, 2013, **5**, 713.
22 X. Bao, L. Sun, W. Shen, C. Yang, W. Chen and R. Yang, *J. Mater. Chem. A*, 2014, **2**, 1732.
23 A. Linsebigler, G. Lu and J. Yates Jr, *Chem. Rev.*, 1995, **95**, 735.
24 K. Kim, S. Cook, S. M. Tuladhar, S. A. Choulis, J. Nelson, J. R. Durrant, D. D. C. Bradley, M. Giles, I. McCulloch and C. S. Ha, *Nat. Mater.*, 2006, **5**, 197.
25 G. Li, Y. Yao, H. Yang, V. Shrotriya, G. W. Yang and Y. Yang, *Adv. Funct. Mater.*, 2007, **17**, 1636.
26 S. Chen, C. E. Small, C. M. Amb, J. Subbiah, T. Lai, S. Tsang, J. R. Manden, J. R. Reynolds and F. So, *Adv. Energy Mater.*, 2012, **2**, 1333.
27 J. K. Lee, W. Ma, C. J. Brabec, J. Yuen, J. S. Moon, J. Y. Kim, K. Lee, G. C. Bazan and A. J. Heeger, *J. Am. Chem. Soc.*, 2008, **130**, 3619.
28 S. Lou, J. M. Szarko, T. Xu, L. Yu, T. J. Marks and L. Chen, *J. Am. Chem. Soc.*, 2011, **133**, 20661.
29 B. Aich, J. Lu, S. Beaupre, M. Leclerc and Y. Tao, *Org. Electron.*, 2012, **13**, 1736.
30 M. Li, L. Wang, J. Liu, K. Zhou, X. Yu, R. Xing, Y. Geng and Y. Han, *Phys. Chem. Chem. Phys.*, 2014, **16**, 4528.
31 M. Pomerantz, *Synth. Met.*, 2003, **135**, 257.
32 Y. Liang, Y. Wu, D. Feng, S. T. Tsai, H. J. Son, G. Li, C. Ray and L. Yu, *J. Am. Chem. Soc.*, 2009, **131**, 56.
33 J. Zhang, W. Cai, F. Huang, E. Wang, C. Zhong, S. Liu, M. Wang, C. Duan, T. Yang and Y. Cao, *Macromolecules*, 2011, **44**, 894.
34 Y. Li, J. Zou, H. Yip, C. Li, Y. Zhang, C. Chueh, J. Intemann, Y. Xu, P. Liang, Y. Chen and A. Jen, *Macromolecules*, 2013, **46**, 5497.
35 J. Cao, W. Zhang, Z. Xiao, L. Liao, W. Zhu, Q. Zuo and L. Ding, *Macromolecules*, 2012, **45**, 1710.
36 X. Bao, T. Wang, A. Yang, C. Yang, X. Dou, W. Chen, N. Wang and R. Yang, *Mater. Sci. Eng., B*, 2014, **180**, 7.
37 K. Vandewal, A. Gadisa, W. Oosterbaan, S. Bertho, F. Banishoeib, I. Severen, L. Lutsen, T. Cleij, D. Vanderzande and J. Manca, *Adv. Funct. Mater.*, 2008, **18**, 2064.
38 M. Drees, H. Hoppe, C. Winder, H. Neugebauer, N. S. Sariciftci, W. Schwinger, F. Schaffler, C. Topf, M. C. Scharber, Z. Zhu and R. Gaudianad, *J. Mater. Chem.*, 2005, **15**, 5158.
39 G. Li, V. Shrotriya, J. Huang, Y. Yao, T. Moriarty, K. Emery and Y. Yang, *Nat. Mater.*, 2005, **4**, 864.
40 J. H. Seo, S. Y. Nam, K. Lee, T. Kim and S. Cho, *Org. Electron.*, 2012, **13**, 570.
41 C. T. Lee and C. H. Lee, *Org. Electron.*, 2013, **14**, 2046.

